Soliton propagation and diffusion of optically excited carriers in beta -rhombohedral boron

1995 J. Phys.: Condens. Matter 7 7851

(http://iopscience.iop.org/0953-8984/7/40/016)

J. Phys.: Condens. Matter 7 (1995) 7851–7870. Printed in the UK

Soliton propagation and diffusion of optically excited carriers in β-rhombohedral boron

Helmut Werheit and Frank Kummer

Solid State Physics Laboratory, Gerhard-Mercator University Duisburg, D 47048 Duisburg, Germany

Received 30 March 1995

Abstract. Drift experiments on optically excited electrons and holes in β-rhombohedral boron in drift of fields up to 146 V cm^{-1} at room temperature show that the propagation of both carriers is of the soliton type. The velocities tend to saturate even at the rather low drift fields used. Characteristic mobilities are $\mu_e = 0.11$ and $\mu_h = 0.076$ cm^2 V^{-1} s^{-1}. Different ratios of the retrapping to the recombination rate, 15 for electrons and 1.2 for holes, are explained by the different modes of action of the electronic states involved. For electrons the mean drift distance between generation and recombination exceeds 3 cm. The representative diffusion constant of electrons and holes $D = 6 \times 10^2$ to 7×10^3 cm^2 s^{-1} depends on the specific conditions. The diffusion covers carrier velocities between 10^{-5} and 10^2 cm s^{-1}. The decay of photoconduction can be exactly described by the re-excitation of trapped electrons and their subsequent recombination.

1. Introduction

Currently β-rhombohedral boron is the model substance of the icosahedral boron-rich semiconductors. Its rhombohedral unit cell has the structural composition $(B_{12})_4(B_{28})_2B$ and contains four B_{12} icosahedra essentially determining its electronic structure (figure 1). Essentials of this energy band scheme—in as far as it is responsible for the electronic transport properties—are, meanwhile, understood: as a consequence of the static Jahn–Teller effect the icosahedra at the vertices of the rhombohedral unit cells are slightly distorted. Electronically in free icosahedra the Jahn–Teller effect leads to the separation of occupied and unoccupied orbitals, and in crystalline icosahedral structures to a low-density split-off valence band (VB1) with localized states. It is positioned 0.188 eV above the actual valence band (VB2) with extended states [1, 2]. Accordingly these solids are semiconductors in spite of the odd number of electrons in the boron atom. Via electron–phonon interactions, a series of six intrinsic electron trapping levels are generated below the conduction band edge at ionization energies which are multiples of 0.188 eV [3, 4, 5].

Until now these complex conditions have prevented the reliable determination of the mobilities of carriers in the different bands [6, 7] (see also [8] and references therein). A first successful attempt at a time-of-flight experiment with drift lengths of several mm allowed the estimation of the mean mobility of the carriers from the ambipolar diffusion [9]. Meanwhile the set-up concerned has been essentially improved, in particular by increasing the signal-to-noise ratio, and our drift experiments on high-purity β-rhombohedral boron at room temperature presented in this paper yield the drift mobilities of electrons and holes and their dispersion.

0953-8984/95/407851+20$19.50

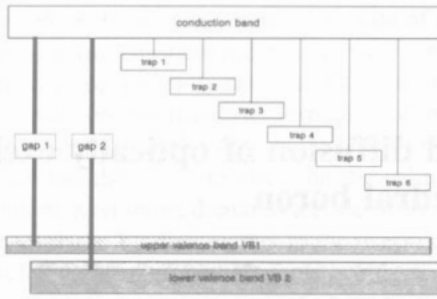

Figure 1. The energy band scheme of pure (β-rhombohedral boron. Gap 1: 1.32(1) eV ($\boldsymbol{E} \parallel \boldsymbol{c}$), 1.29(1) eV ($\boldsymbol{E} \perp \boldsymbol{c}$), gap 2: 1.50(1) eV ($\boldsymbol{E} \parallel \boldsymbol{c}$), 1.46(1) eV ($\boldsymbol{E} \perp \boldsymbol{c}$); the values are extrapolated to $T = 0$ K. Position of electron traps: n times 0.188(2) eV ($n = 1$ to 6) below the conduction band edge [1–5].

2. Sample material and experimental set-up

From high-purity β-rhombohedral boron single crystals (Wacker, Munich; claimed purity 99.9999% besides carbon (typically 60 ppm)) a prismatic sample of length 10.26 mm and cross section 1.2 times 1.18 mm^2 was cut roughly parallel to the crystallographic c axis and prepared according to [10]. As probes, thin platinum wires were fixed pairwise on opposite side faces by capacitor discharge, forming a low-melting Pt–B eutectic. This procedure proved to yield ohmic contacts.

Electron–hole pairs are optically generated at one end face of the sample by the radiation of a GaAlAs luminescence diode (880 nm, half-width 80 nm, 50 mW) essentially within the penetration depth of 0.25 mm. Depending on the sign of the drift field, excess electrons or holes are driven through the sample, and their time-dependent concentration modifies the resistance between the particular probe pairs at 1.49, 2.72 and 4.36 mm from the illuminated surface. The change of resistance was determined by detuning a Wheatstone bridge. The noise of this signal could be essentially reduced by electronically subtracting the previously separated AC components from the total signal. The resulting difference signal was registered by a digital storage oscilloscope (Tektronix 2430), which was connected to a personal computer to store the data. In contrast to usual time-of-flight measurements, a steady-state—not pulsed—excitation is used. The oscilloscope is triggered by the onset of the optical excitation.

The resistances of the paths between the probe pairs with and without optical excitation differ by less than 1%. Accordingly the change of the resistance can be essentially attributed to the change of the carrier densities.

3. Experimental results

The change of the resistances as measure of the change of carrier densities at the three probe pairs were determined for the drift fields 0, $\pm$48.7, $\pm$97.5 and $\pm$146 V cm^{-1}. As examples, in figures 2(a)–(c) the spectra for -146, 0, and $+146$ V cm^{-1} show the drift of electrons, the ambipolar diffusion of electron–hole pairs and the drift of holes.

At first sight the drift spectra of electrons and holes and the ambipolar diffusion spectrum of electron–hole pairs in figures 2(a)–(c) appear very similar, showing that diffusion remains the prevailing transport in the drift fields used. Nevertheless, certain qualitative differences can be distinguished even without quantitative evaluation. While conductivity increases

as expected in the case of electron drift, in the case of hole drift the thermal equilibrium conductivity is partly quenched. This quenching increases with drift voltage and increasing distance from the illuminated surface. Within the period of measurement, limited to three hours, saturation of the carrier densities was reached for holes and largely for electron–hole pairs as well. In contrast, the density of electrons is far from being saturated within this period.

In figure 3 the initial range of hole drift is shown in more detail. As an example of the decay density of the excess carriers approaching thermal equilibrium after the exciting light was switched off, the preceding ambipolar drift of electron–hole pairs (drift field strength 0 V cm^{-1}) is shown in figure 4.

4. Verification of the energy band scheme

The energy band scheme of β-rhombohedral boron (figure 1) can be checked by the decay of the photoconduction. After the exciting light is switched off, the excess carrier concentration is decreased by recombination at an enhanced rate until thermal equilibrium is re-established. Through detailed investigation of photoabsorption and photoconductivity [8, 11] it is known that thermal re-excitation of the electrons from the traps into the conduction band is a prerequisite for recombination, while direct transitions of trapped electrons into the valence band can be largely excluded. Hence the time dependence of the decay is expected to be determined by the ionization energies δE_i of the different occupied traps of density n_i according to

$$n(t) = \sum_i n_i e^{-t/\tau_i} \tag{1}$$

with

$$\tau_i \propto e^{-\delta E_i/k_B T}. \tag{2}$$

The n_i and τ_i were determined by plotting $n(t)/n(t=0)$ on a logarithmic scale versus t and by decomposing the different processes as usual i.e. by subtracting the fitted linear slopes step by step from the measured or the remaining values. Within the accuracy of measurement the results depend neither on the kind of drifted carriers, nor the drift field strength, nor the probe position. The averaged results obtained are listed in table 1.

Table 1. Parameters of the decay of excess carriers (electrons and holes) derived from several runs at different drift field strengths with standard deviations.

i	τ_i (s)	n_i (relative units)
1	7.3 ± 1.6	0.20 ± 0.09
2	94 ± 15	0.30 ± 0.07
3	670 ± 95	0.30 ± 0.05
4	8800 ± 1100	0.30 ± 0.06

The agreement between the measured decay and the calculation based on the parameters in table 1 is exemplary as demonstrated in figure 4. The correlation between decay time constants and trap ionization energies according to relation (2) is confirmed in figure 5. Obviously the densities of occupied electron traps with the ionization energies δE_i ($i = 2$ to 4) are the same within the accuracy of measurement. Only the level with $\delta E_1 = 0.188$ eV, situated closest to the conduction band, has a density which is probably somewhat lower.

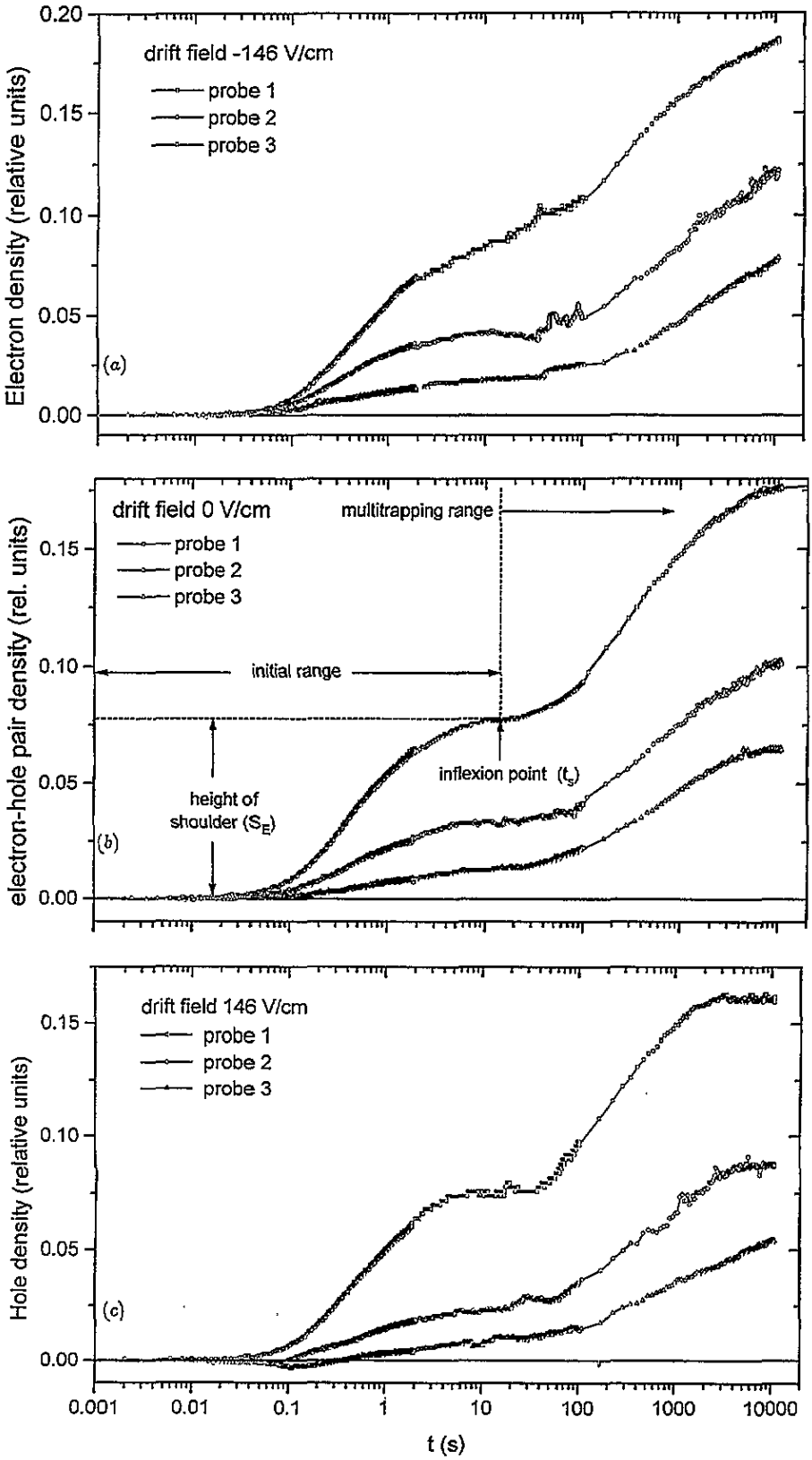
drift field -146 V/cm
probe 1
probe 2
probe 3
Electron density (relative units)
0.20
0.15
0.10
0.05
0.00
(a)
drift field 0 V/cm
multitrapping range
probe 1
probe 2
probe 3
initial range
inflexion point (t_s)
height of shoulder (S_E)
electron-hole pair density (rel. units)
0.15
0.10
0.05
0.00
(b)
drift field 146 V/cm
probe 1
probe 2
probe 3
Hole density (relative units)
0.15
0.10
0.05
0.00
(c)
0.001
0.01
0.1
1
10
100
1000
10000
t (s)

Figure 2. (*Facing page.*) Representative densities of optically excited carriers at the probe pairs 1, 2 and 3 depending on transit time for the drift fields 0 and ±146 V cm^{-1}. The detuning voltage of the Wheatstone bridge is used as measure of the density of carriers: (a) electrons (drift field −146 V cm^{-1}); (b) electron–hole pairs (drift field 0 V cm^{-1}); (c) holes (drift field 146 V cm^{-1}) dependent on time. Notations for specific regions and points of the spectra as used in the paper are is given in figure 2(b).

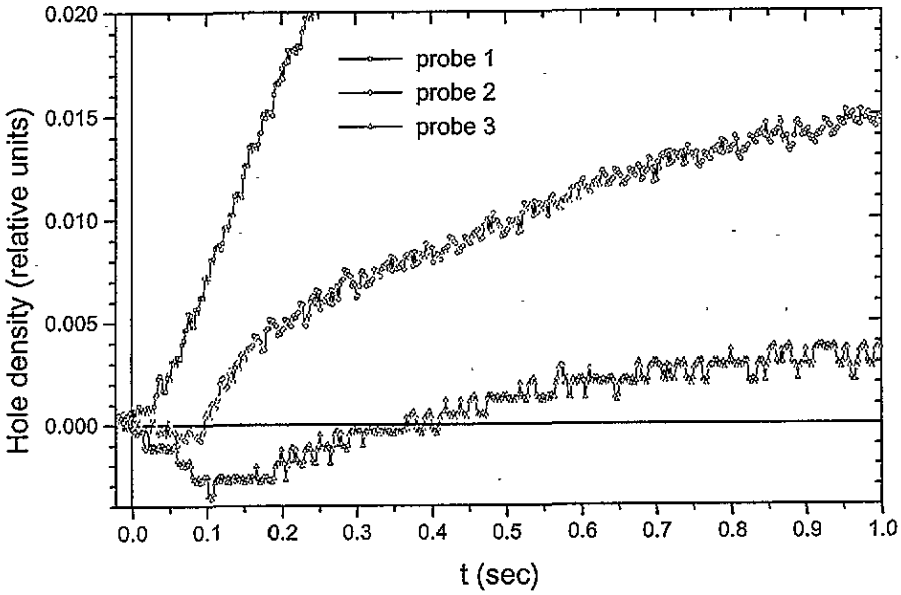

Figure 3. The negative photoconduction at probe pairs 1,2 and 3 in the case of hole drift (drift field 146 V cm^{-1}).

5. Evaluation

All the dispersion spectra obtained exhibit distinct shoulders obviously separating faster and slower carriers. Similar transit dispersion profiles have been measured by Fisher and Willock [12] on one-dimensional polymer single crystals using drift fields which are about 100 times higher than ours. They attribute the shoulder in the dispersion curve to non-uniform drift fields. This interpretation can be excluded for boron as the shoulder occurs without a drift field as well.

Theories describing the non-linear dependence of the transit time on the drift length in time-of-flight experiments, when the dispersion is influenced by traps, were developed by Scher *et al* [13, 14] Schmidlin [15] and Movaghar *et al* [16]. To adapt our spectra obtained by steady-state optical excitation to the theories on pulsed excitation, it is only necessary to take the time-dependent difference between the measured spectra and the particular saturation values. Compared with pulsed time-of-flight experiments our results have the advantage that different drift distances can be investigated with in one sample. A further advantage is that the small initial currents are directly measured and need not be calculated as the uncertain small deviations from noisy saturation values; certainly this advantage reverses at very long drift times. Indeed, theories which are based on an energetical two-band scheme do not contain the hole quenching observed in boron.

Schmidlin's theory and model calculations lead to distinct shoulders in dispersion spectra

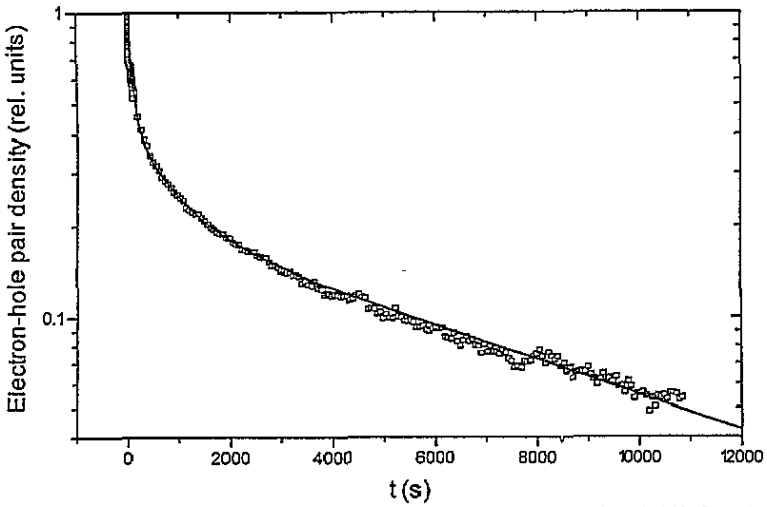

Figure 4. An example of decay of the photoconduction for probe 1 and drift field 0 V cm^{-1} (ambipolar diffusion of electron–hole pairs). The fitted curve was calculated according to equation (1) with the parameters in table 1.

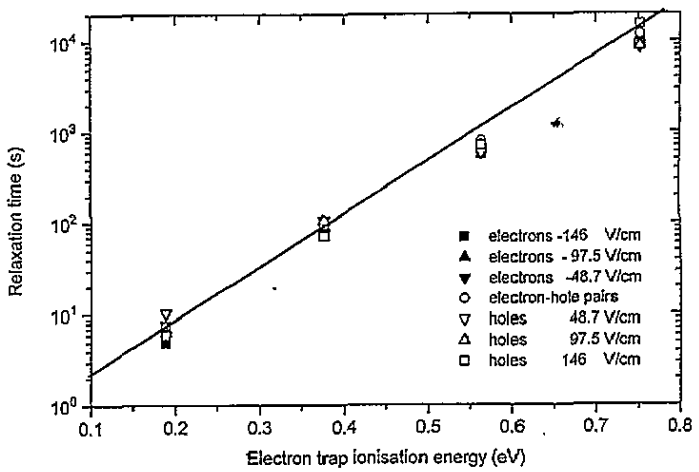

Figure 5. Relaxation time constants of the excited carriers versus electron trap ionization energies according to relation (2).

like those in figure 2(a)–(c). He attributes the initial range limited by the shoulder to the microscopic mobility of largely untrapped carriers in the extended states of the energy bands where the dispersion is determined by diffusion. The dispersion in the second range extending from the shoulder to the saturation value approached asymptotically is determined by multiple trapping and thermal re-excitation of the trapped carriers. The specific slope depends on the energetical positions of the trapping levels involved in the transport. However, when the time at which the shoulder is reached in Schmidlin's model calculations for typical untrapped carriers is compared with the inflexion points t_s in the shoulders of the spectra in figures 2(a)–(c), it is obvious that this concept cannot be immediately transferred to β-rhombohedral boron. Nevertheless, as will be shown below, Schmidlin's theory can be usefully adapted to our experimental results when (i) the initial

range is attributed to carriers whose transport is influenced, for example, by statistical trapping in more or less shallow traps being in thermal exchange with the associated energy band, and (ii) the final range is attributed to multi-trapping in deep traps.

5.1. Trapping and recombination

To compare the dispersion spectra obtained at probes at different distances from the illuminated surface quantitatively, it is necessary to take the loss of mobile carriers by trapping and recombination into account, both increasing with increasing drift length. In the initial range, which is essentially limited by the shoulder, losses via interband recombination or trapping events cannot be distinguished, whilst in the final steady state only the interband recombination is relevant. In both cases the slope is determined by a characteristic decay time constant τ_i and a characteristic drift length L_i respectively according to

$$n/n_0 = \exp(t\tau_i) = \exp(tv_0/\tau v_0) = \exp(L/L_i). \tag{3}$$

Table 2. Experimentally determined heights of the shoulders S_E , and times of inflexion points t_s within the shoulder.

Carrier type	Drift field E_D (V cm^{-1})	Probe pair 1 (l = 1.49 mm) S_E	t_s (s)	Probe pair 2 (l = 2.72 mm) S_E	t_s (s)	Probe pair 3 (l = 4.36 mm) S_E	t_s (s)
Electrons	−146	0.093	8.6	0.0416	9.5	0.0176	11
	−97.5	0.086	11.7	0.0392	8.3	0.0160	7.1
	−48.7	0.075	7.4	0.0332	7.1	0.0142	7.4
Electron–hole pairs	0	0.077	6.7	0.0337	8	0.0124	8.7
Holes	48.7	0.0818	9.9	0.0293	6.6	0.0129	8.2
	97.5	0.0758	5.7	0.0227	6.5	0.00908	8.4
	146	0.0758	7.3	0.0229	8.5	0.0103	10.25

To characterize the loss via recombination and trapping in the initial range both $1/L_{initial}$ $(= 1/L_{recombination} + 1/L_{trapping})$ the heights of the shoulders S_E (table 2) are logarithmically plotted versus the drift length L for holes in figure 6, and for electrons in figure 7(a). The extrapolations to zero distance yield the densities at the illuminated surface. The corresponding slope of the saturation values yields $L_{recombination}$ (mean drift length between generation and interband recombination) determined by recombination only. The relation of trapping and recombination probabilities $P_{trapping}$ and $P_{recombination}$ for holes is:

$$\frac{P_{trapping}(\text{holes})}{P_{recombination}(\text{holes})} = \frac{L_{recombination}}{L_{trapping}} = 1.2(1).$$

Determination of $L_{recombination}$ for the electrons requires the estimation of the saturation values not reached within the period of measurement. Two attempts are shown in figure 7(b). If full saturation is supposed to be reached at the first probe, the saturation values at larger distances result from extrapolation of the slope determined by the surface density (which is in turn determined by extrapolation in figure 7(a)), and the first-probe value to larger distances. However, these values can be taken as lowest limits only, because the spectra indicate that saturation even at the first probe is not yet established within the measuring period. For a more reliable estimation of $L_{recombination}$ the saturation value at the first probe

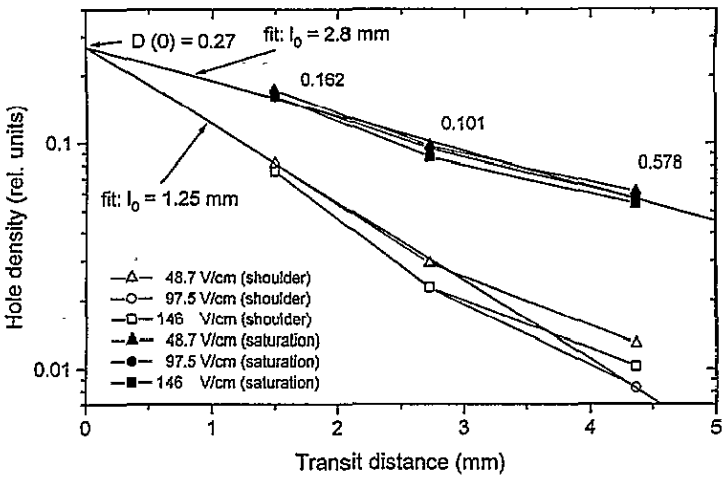

Figure 6. The decay of the hole concentration depending on the distance from the illuminated surface: ▲, △48.7 V cm^{-1}; ○, ● 97.5 V cm^{-1}; □, ■ 146 V cm^{-1}; open symbols—heights of the shoulders S_E (see table 2), with decay due to both interband recombination and trapping processes both; solid symbols—(saturation values at the probe pairs), with decay due to interband recombination only. The recombination time constant was calculated according to equation (3).

was approximated by empirical exponential extrapolation, and subsequently the saturation values at larger distances were obtained by extrapolation as described. The results are listed in table 3. The resulting ratio of the trapping and recombination probabilities for electrons is much larger than for holes:

$$\frac{P_{trapping}(\text{electrons})}{P_{recombination}(\text{electrons})} = \frac{L_{recombination}}{L_{trapping}} = 15(4).$$

Table 3. Characteristic drift lengths of carriers in β-rhombohedral boron ($L_{trapping}$ denotes the mean drift distance between generation and trapping, $L_{recombination}$ the mean distance between generation and interband recombination). The drift field dependence could not be reliably determined for holes. For electrons the results of two different procedures (see the text) are given; the less probable ones are in brackets. $L_{trapping}$ was calculated from $L_{initial}$ and $L_{recombination}$.

		Characteristic drift lengths of carriers			
			$L_{recombination}$ (mm) derived from saturation at probe 1		
Carrier type	E_D (V cm^{-1})	$L_{initial}$ (mm) derived from shoulder	Saturation assumed	Saturation extrapolated	$L_{trapping}$ (mm)
Electrons	0	1.53	(11.0)	13.5(5)	1.7
	−146	1.75	(17.5)	35(4)	1.8
Holes	146	1.25	2.8	—	2.3

The characteristic drift lengths increase with the increasing drift field strength as expected, because trapping and recombination probability decrease with increasing velocity. While for holes $L_{recombination}$ is comparable to that for classical semiconductors, for electrons $L_{recombination}$ far exceeds these values. The reason for this difference will be discussed below.

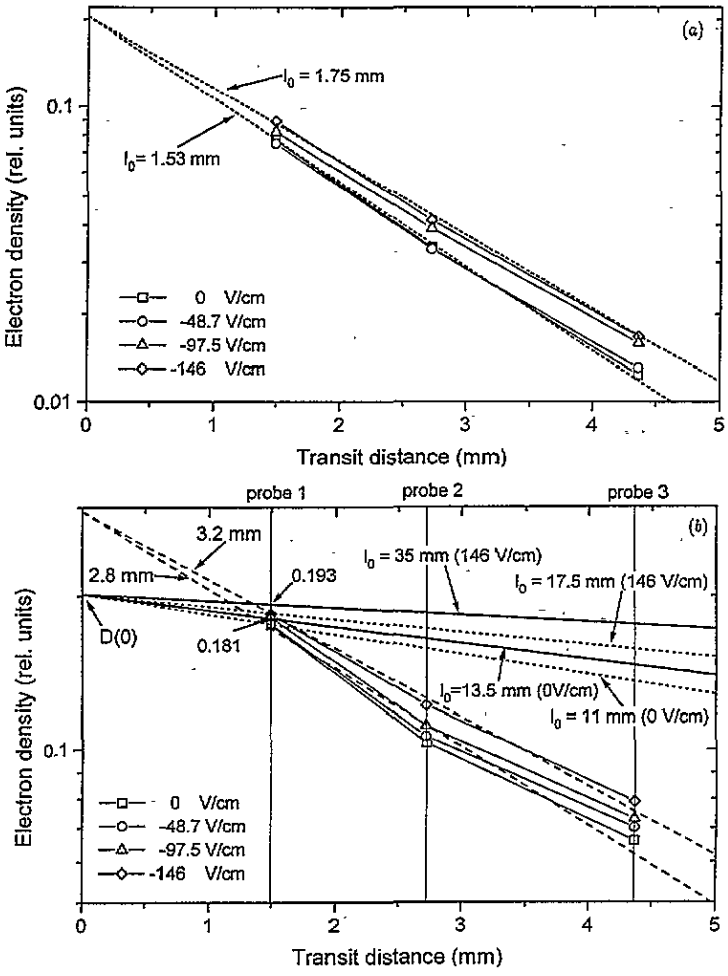

Figure 7. The decay of the electron concentration depending on the distance from the illuminated surface: □, 0 V cm^{-1}; ○, −48.7 V cm^{-1}; △, −97.5 V cm^{-1}; ◇, −146 V cm^{-1}. (a) The decay due to both interband recombination and trapping processes; open symbols—(heights of the shoulders S_E (see table 2). (b) The decay due to interband recombination only. Density $D_{(0)}$ was obtained from figure 7(a). Dotted line—saturation at probe pair 1 assumed, values for larger transit distances obtained by extrapolation; solid line—saturation value $D_{extrapol}$ (1) at probe 1 obtained by extrapolation, values for larger drift distances determined by extrapolation from $D_{(0)}$ obtained from figure 7(a) and $D_{extrapol}$ (1) (for details, see the text and results given in table 1).

5.2. Drift of electrons and holes

At first viewing the quenching of the equilibrium conductivity in the initial range of hole drift is striking. However, on the basis of the energy band scheme in figure 1 it can be easily explained. At room temperature the electrical conductivity of β-rhombohedral boron is essentially determined by hopping processes within the upper valence band. The photons of 1.41 eV energy used for excitation raise electrons from this upper valence band into the conduction band (E_g = 1.29/1.32 eV) but not from the lower valence band (E_g = 1.46/1.50 eV). Hence the electron density in the upper valence band, which is responsible for these hopping processes is progressively reduced by the optical excitation

increasing the number of excited holes reaching the probe pair. The sign reverse at longer times can be explained accordingly. As is known from optical absorption [4], the quasi-Fermi level within the upper valence band is lowered even in cases of moderate optical excitation because of the low density of states. Accordingly the minimum activation energy for high-mobility holes in the lower valence band decreases, their contribution to the conductivity finally prevails, and the photoconduction changes to positive values as compared with the thermal equilibrium conductivity.

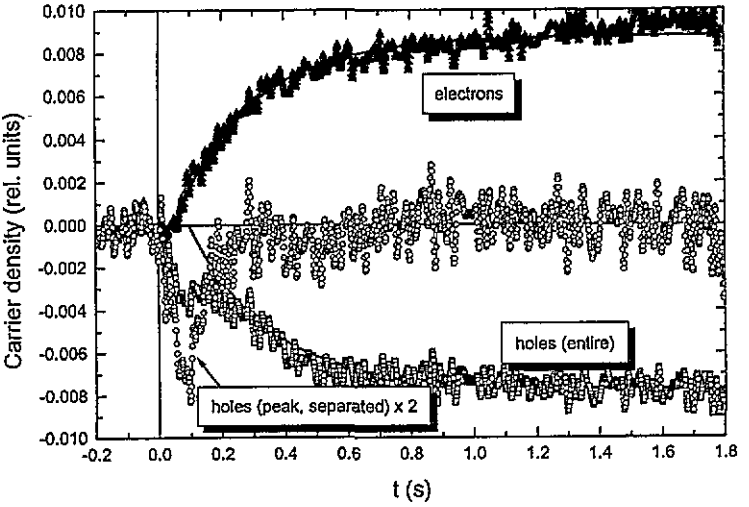

Figure 8. Densities of drifting electrons and holes depending on transit time (representative for probe 2, $E_D = \pm 146$ V cm^{-1}). The separated hole peak is enlarged by a factor of 2.

As can be obtained from figures 2(a)–(c) the contribution of drift to the dispersion spectra is small compared with that of diffusion. However, the drift results can be approximately separated out as the difference between the spectra with and without drift fields applied. As an example, in figure 8 it is shown that apart from being of opposite sign the dispersions of the drift spectra of electrons and holes differ qualitatively.

The drift-enhanced electron density begins at a certain minimum time indicating the maximum drift velocity and exponentially approaches a saturation value. At longer times the drift of holes approaches saturation exponentially as well; however, at small drift times a distinct maximum is superimposed, which can be empirically described by a Gaussian distribution multiplied by time t to realize zero contribution at $t = 0$. The drift times of electrons and holes obtained from specific points in the dispersion spectra at the different probes (onset for electrons, peak maximum for holes) scale linearly with the drift distance (figure 9) showing that the drift velocities are independent of drift length.

The field dependences of the drift velocities tend to saturation even for the rather low drift fields used (figure 10(a)). The carrier mobilities have been determined from the initial tangents of the fitted slopes (table 4). While $\mu_e = 0.11$ cm^2 V^{-1} s^{-1} is the maximum electron mobility, the mobilities $\mu_h = 0.076$ and 0.14 cm^2 V^{-1} s^{-1} correspond to the maximum and the half- maximum probability of drifting holes within the peak (figure 11). Within the accuracy of these measurements there is a non-zero probability of drifting holes up to the electronically determined resolution limit of the set-up of at least 400 cm^2 V^{-1} s^{-1}.

Assuming [17] that the field dependence of the drift velocity is caused by a field-

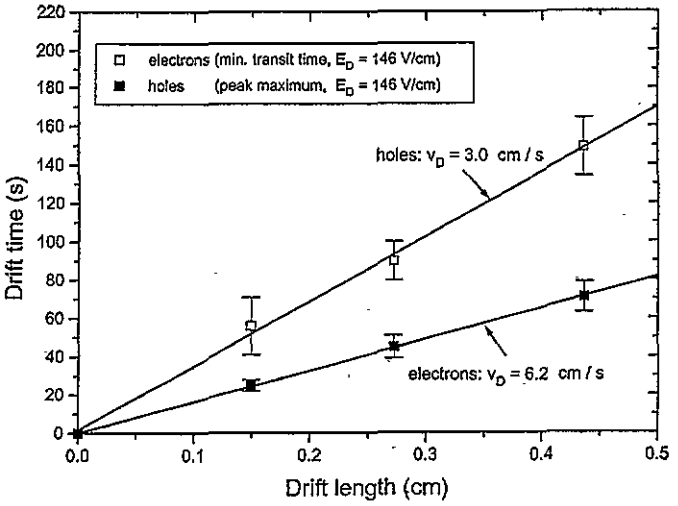

Figure 9. Drift times of electrons and holes at specific points of the dispersion spectra versus drift length.

Table 4. Drift mobilities of electrons and holes at specific points of the dispersion spectra.

Carrier type	Mobility ($cm^2\ V^{-1}\ s^{-1}$)	Characterization
Electrons	0.11	From minimum drift time (initial point)
	0.068	Intersection between initial tangent and extrapolated saturation
	0.074	From time at the half-saturation point
Holes	0.076	At peak maximum
	0.14	At half-maximum point of the peak

dependent trap release time:

$$\tau_b = (A/E_D)\exp(\Delta E/kT)$$

with the constant A independent of temperature and drift field E_D, and ΔE, the activation energy of the traps, Fisher and Willock [12] have shown that the drift velocity v_d varies as

$$V_D = \frac{1}{[1/V_0 + (C/E_D)\exp(\Delta E/k_T)]} \tag{4}$$

with $C = NA/L$ and N the number of traps of energy ΔE sampled by the faster carriers in the drift length L. The plot of $1/v_D$ versus $1/E_D$ (figure 10(b)) shows that this equation can be applied to boron as well. However, the maximum velocities

$$v_0(\text{electrons}) = 11\ \text{cm s}^{-1}$$
$$v_0(\text{holes}) = 4\ \text{cm s}^{-1}$$

obtained for $E_D \to \infty$ by extrapolating $1/E_D \to 0$, where the trap release times tend towards zero, are far from the sound velocity of β-rhombohedral boron $v_S = 1.4 \times 10^6$ cm s^{-1} [18]. Hence, in spite of the formal similarity of the slope, the transport mechanism in β-rhombohedral boron is qualitatively different from the solitary-wave acoustic polarons (SWAP) in one-dimensional polymers [12].

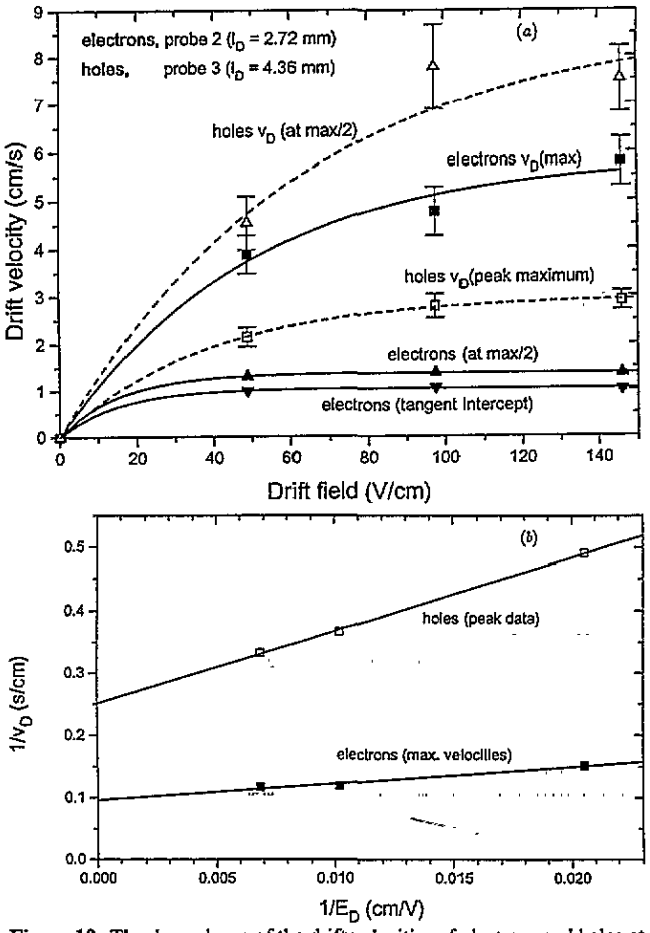

Figure 10. The dependence of the drift velocities of electrons and holes at specific points of their dispersion spectra. (a) Drift velocity versus drift field. The initial tangents yield the mobilities listed in table 4. (b) Reciprocal drift velocity versus reciprocal drift field according to equation (4). Extrapolation to $1/v_D = 0$ yields the maximum velocities 11 cm s^{-1} for electrons and 4 cm s−1 for holes.

Nevertheless, the soliton-type propagation of drifting carriers in β-rhombohedral boron is obvious. The empirical fits of the electron dispersion spectra for 146 V cm^{-1} drift field and their derivatives in figure 12 show that the carrier front, which propagates with the velocity given in table 4, steepens considerably with increasing drift length. When the reduction of carrier concentration by trapping and recombination shown in figure 7 and 8 is taken into account, this effect becomes even more pronounced. The qualitative reason for the nonlinear drift velocity as a prerequisite for the development of solitons is that a fraction of the electrons drifting ahead is captured in traps and reduces the trapping probability for the following electrons, whose velocity increases accordingly.

In the case of holes a solitary wave seems to develop. Figure 11 shows the peak separated from the total dispersion spectrum as indicated above. Its area, apparently broadened by diffusion, increases exponentially with drift time and increasing drift distance. To explain the non-linearity of the hole velocity, two models seem possible at present. (i) The number of electrons in the upper valence band is reduced by the holes drifting from

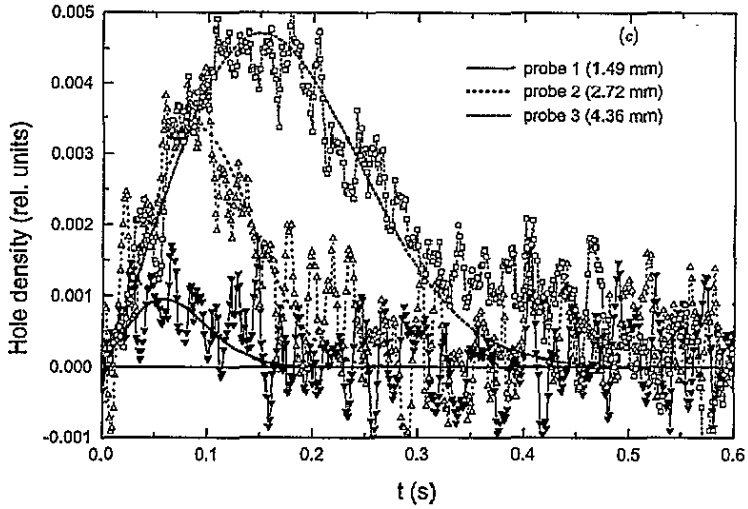

Figure 11. The density distribution of drifting holes at different distances from the illuminated surface within the front peak separated from the total drift spectrum of the holes (E_D = 146 V cm^{-1}). The fitting curves are empirically calculated using Gaussian distribution times t to realize zero density at $t = 0$.

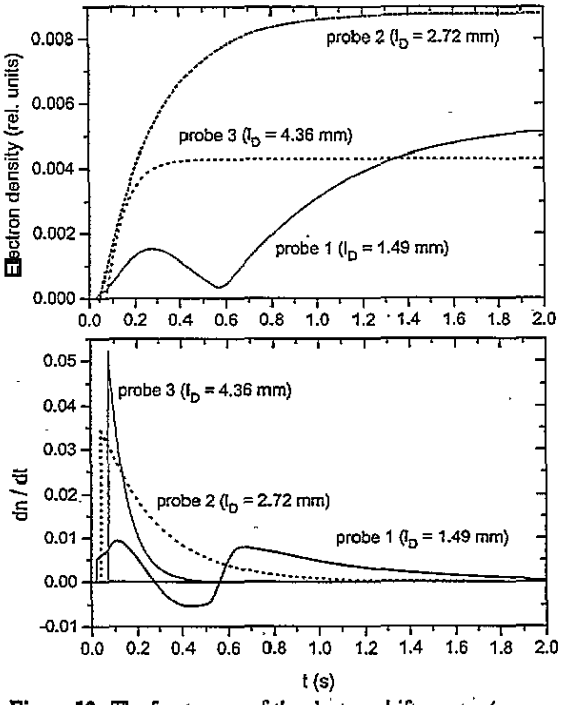

Figure 12. The front range of the electron drift spectra (representative for $E_D = -146$ V cm^{-1}) versus transit time for differing distances from the illuminated surface. (a) Empirical fits to the spectra measured (decay of electron density by recombination has not been considered). (b) Derivatives of the curves in figure 12(a).

the illuminated surface. Accordingly the quasi-Fermi level, which is assumed to be in the upper part of the upper valence band, is slightly lowered and moves into a range with higher density of states and correspondingly higher hopping probability. However, this interpretation seems to contradict the negative sign of the photoconduction in the initial range. (ii) If the transport preferential takes place via free holes in the lower valence band, and the occupied states in the upper valence band act as hole traps, the decreasing occupation density of the upper valence band is equivalent to a decreasing density of effective hole traps, leading to a drift velocity of the high-mobility holes in the lower valence band VB2 that increasing with time. This interpretation seems to be more consistent with the other results.

5.3. Diffusion

Since the contribution of diffusion to the complete dispersion spectra is dominant, the dispersion of the carriers can be determined to a good approximation by Fick's second law

$$\frac{\partial n}{\partial t} = -Dq\frac{\partial^2 n}{\partial x^2}. \tag{5}$$

For the boundary condition of a time-independent concentration at the illuminated front the solution of this equation is

$$n(t, x) = n_0(1 - \Psi(\xi))$$

with the Gaussian error function

$$\Psi(\xi) = \frac{2}{\sqrt{2\pi}}\int_0^{\xi} \exp(-u^2)\,du$$

where

$$\xi = \frac{x}{2\sqrt{Dt}}.$$

In figure 13 the diffusion constants D are plotted versus the degree of approximation to the saturation in the shoulder. D increases with increasing drift length. The essential reason is assumed to be the soliton-type propagation of the carriers leading to their accumulation at higher velocities.

For those carriers whose capture times are small compared with their transit times a Gaussian velocity distribution is expected. Since for stationary excitation the values of the dispersion spectra at t_X are averages over those for all carriers with drift times $t < t_X$, the derivative with respect to time yields a carrier density depending on t_X. A Gaussian distribution was found for drift times $t_X < 1$ s. Attributing the specific diffusion constant to the maximum of these Gaussian distributions one gets from figure 13, depending on the specific conditions, $D = 6 \times 10^2$–7×10^3 cm^2 s^{-1}.

As emphasized by Schmidlin [15], the validity of the Einstein relation $D/\mu = kT/e$ is restricted to carrier transport in extended states without trapping and therefore it is not applicable to boron. However, the values for μ and D derived from experiment allow us to check the dispersion measured according to Schmidlin's theory. Since this theory is based on pulsed excitation, the experimental data must be related to the relative saturation value within the shoulder. Schmidlin's equation (B7) corresponds exactly to the conditions in the initial range of dispersion, determined by drift and diffusion, when multitrapping can be excluded:

$$I(t) = A\exp(-\omega_0 t)\left\{1 - \int_0^t Y_D(t)\,\mathrm{d}t\right\}. \tag{6}$$

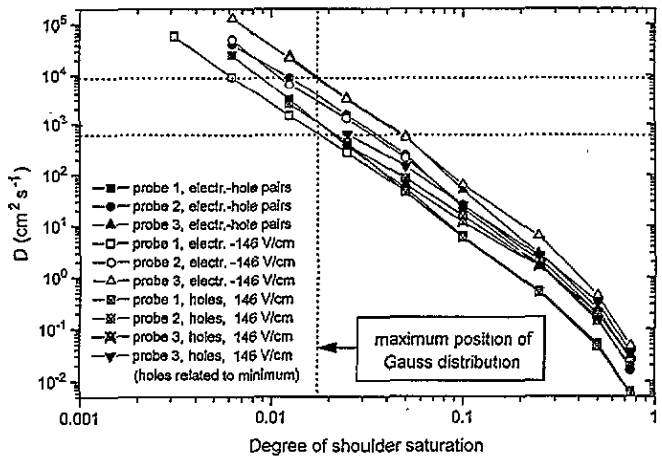

Figure 13. Dispersion of the diffusion coefficients of the carriers in the initial range of propagation for different probes and drift fields. The data are plotted versus the degree of approximation to the carrier density at the inversion point of the shoulder in the dispersion spectra.

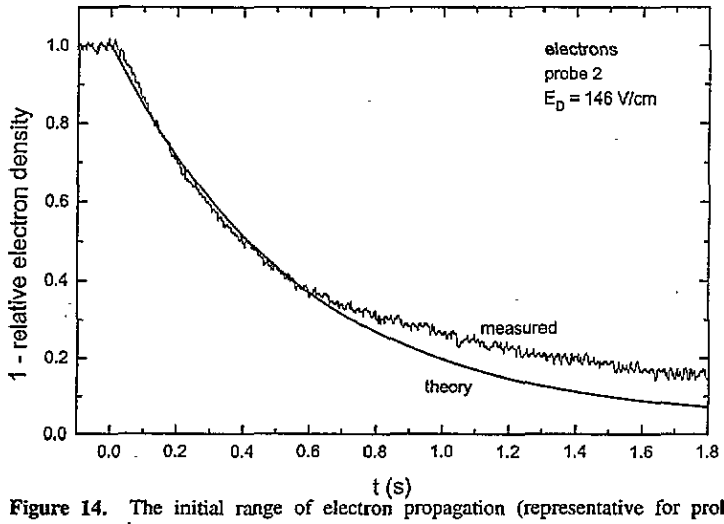

Figure 14. The initial range of electron propagation (representative for probe 2, $E_D = -146$ V cm^{-1}) plotted according to Schmidlin's theory of pulsed excitation [15] (see the text). The solid line, shows the fit from equation (6).

The prefactor with $A = (q\eta N_0 \mu E_D)/L$, where q is the charge of the carriers, N_0 is the total number of nonreflected photons, η is the quantum yield, L is the drift distance, μ is the carrier mobility, and E is the drift field strength, is experimentally determined by the height of the shoulder. $\omega_0 = N_i \sigma \mu E_D$ contains N_i, the density of trapping centres and σ_i their capture cross section.

$$Y_D(t) = \frac{1}{\sqrt{2\pi}\sqrt{(2DL)/(\mu E_D)^3}} \exp\left[\left(t - \frac{L}{\mu E_D}\right)^2 \Big/ \left(4D\frac{L}{(\mu E_D)^3}\right)\right]$$

describes the dispersion in transit times resulting from diffusion. Figure 14 shows that the calculation with the experimentally determined parameters $D = 2000$ cm^2 s^{-1} and

$\mu = 10^{-1}$ cm^2 V^{-1} s^{-1} fits the experimental slope quite well in the initial range. For the only free parameter to fit the theoretical curve, $M = N_t\sigma_i = 0.075$ is used. The deviation towards longer times is probably due to the increasing dispersion caused by re-excitation from traps, which has a certain probability for these comparably long drift times.

5.4. Dispersion of the carrier velocities

To determine the complete dispersion of the carrier transit times the lifetimes and the mean drift distances between optical generation and interband recombination are relevant, irrespective of how long or how often these carriers may have stayed in traps during their individual transit times. Accordingly, to compare the spectra obtained at different distances, it is necessary to eliminate the distance-dependence decay caused by recombination by relating the spectra to the respective saturation values (table 2).

In figures 15(a) and (b) the accordingly modified transit time spectra for electrons and holes obtained at drift fields of 146 V cm^{-1} are shown. Beyond the shoulder the velocity of the carriers is essentially determined by multitrapping. It is obvious in the case of the holes, and indicated in the case of electrons in spite of the restricted range, that in the multi-trapping range the slopes of the spectra at different distances from the illuminated surface are largely parallel. Because of the logarithmic timescale this means that the velocity distributions of the carriers are largely independent of the transit time. Obviously in this range the density of holes decreases exponentially with velocity increasing. For the electrons the slope deviates progressively from this behaviour with the transit time increase.

The parallel slope of the dispersion spectra suggests that we can calculate the velocities of the carriers as the ratio of distance from the illuminated surface to the transit time. However, the resulting velocity distributions in the multi-trapping range (figure 16) depend on distance. To discover the reason for this, the slopes in the multi-trapping range of figures 15 were extrapolated to the abscissa to get comparable relative shifts of the spectra. In the case of the electrons the initial tangents beyond the shoulders were taken for this extrapolation. Figure 17 shows that within the accuracy of measurement these shifts are proportional to the distance from a point 1.25 mm away from the illuminated surface. Apparently the carriers move quickly within this initial range of 1.25 mm, and then they adopt largely uniform small velocities determined by statistical multi-trapping. We fairly safely assume that this is not caused by optical excitation in the volume, because 1.25 mm exceeds the penetration depth (0.25 mm). We assume that the traps in the initial drift range have become largely saturated, and accordingly the trapping probability decreases. Such behaviour would certainly be better explained by drift times exponentially increasing with the distance from the illuminated surface, and figure 17 shows that the corresponding fit is satisfactory as well. For a reliable explanation of this effect additional measurements are necessary.

From the dispersion spectra in figures 16(a) and 16(b) representing the integrals of carriers with velocities higher than indicated by the specific abscissa values, the derivative was determined as a measure of the density distribution of the carriers depending on the velocity. The untrapped and multi-trapped holes are more distinctly separated than the electrons. Besides the variety of electron traps—compared with only one hole trap (figure 1)—the reason could be that additional, shallower levels exist close to the conduction band. FIR optical investigations have already led us to assume the existence of such levels.

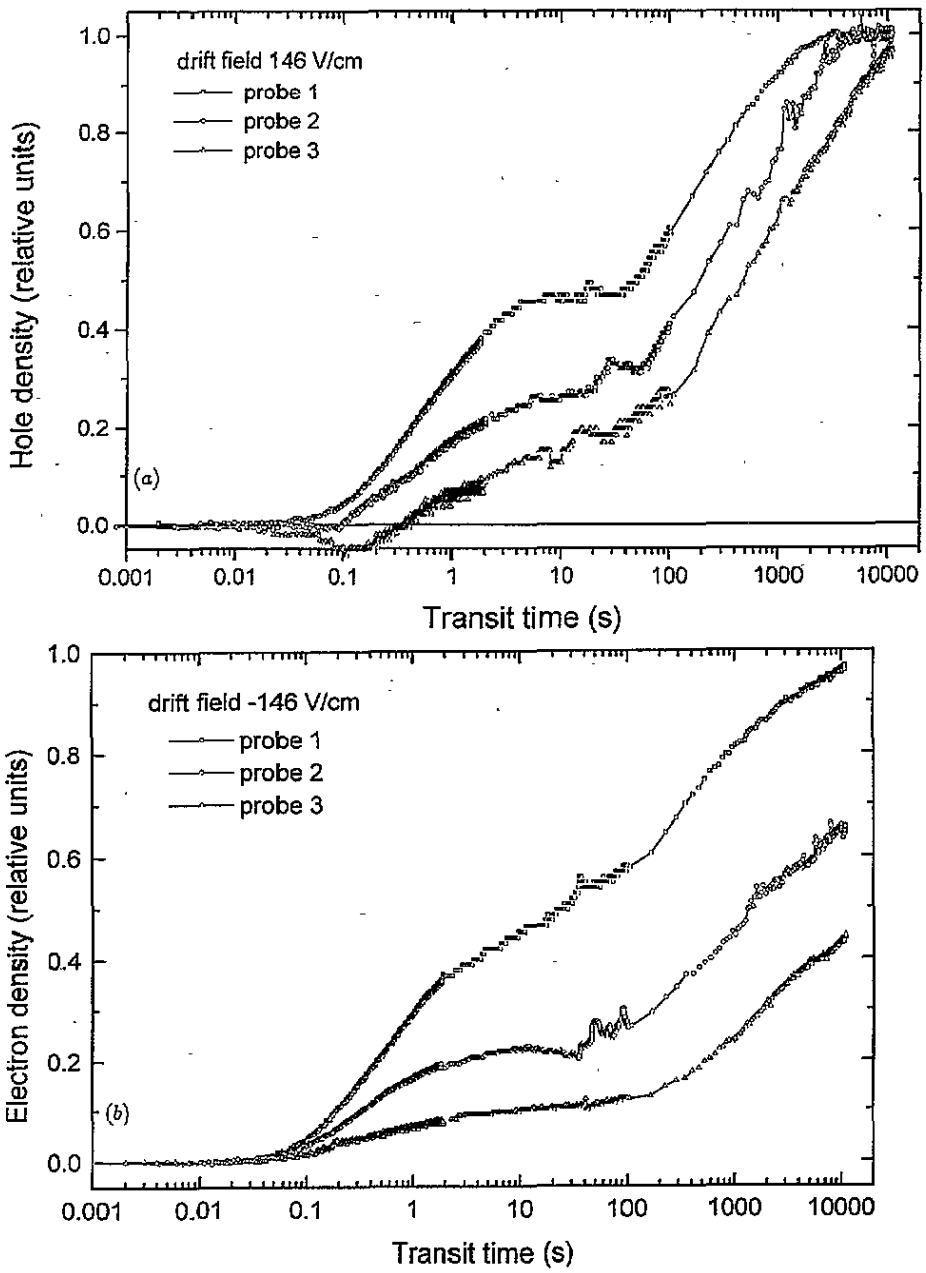

Figure 15. Excess carrier densities versus transit time normalized to the respective saturation values (see figures 2(a)–(c)) to eliminate the loss by recombination. (a) Holes. (b) Electrons.

6. Summary

For electrons and holes in β-rhombohedral boron drift mobilities of the order of 10^{-1} cm^2 V^{-1} s^{-1} were determined for drift lengths between 1.49 and 4.36 mm. Since the traps for electrons and holes are generated by the interaction of electrons and intra-icosahedral phonons the mean distance between traps is roughly of the order of the distance

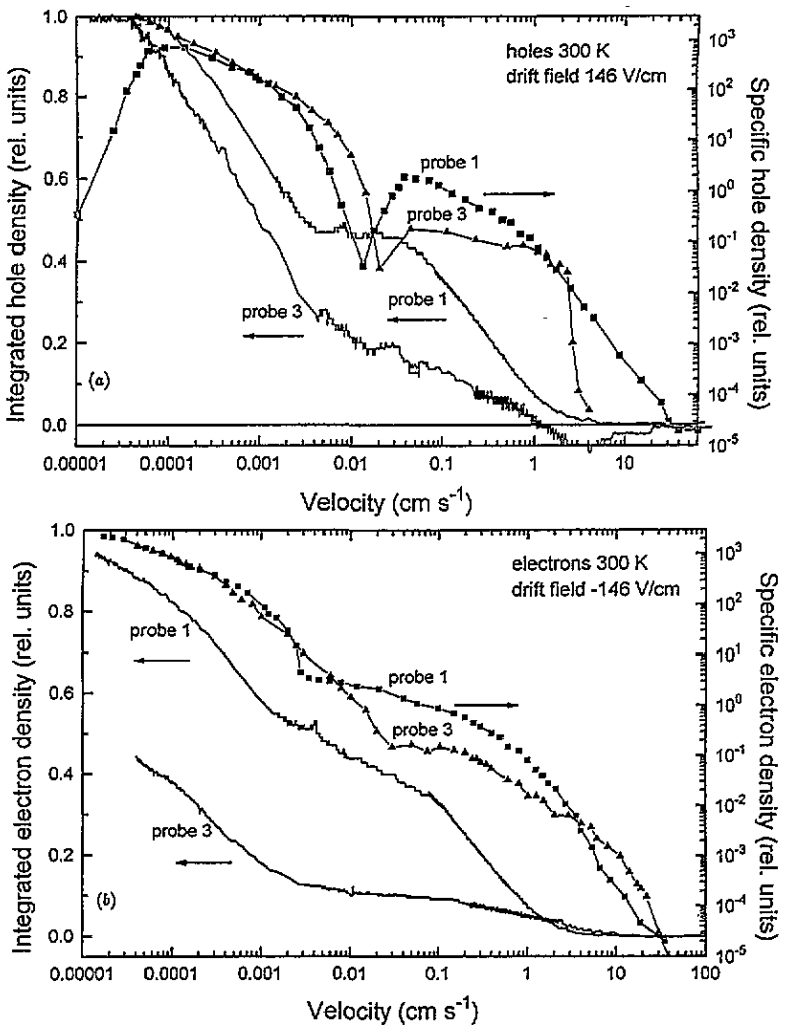

Figure 16. Integrated carrier densities measured (solid lines) and specific carrier densities (symbols) determined as derivatives with respect to time at probes 1 and 3 versus mean velocity between the illuminated surface and the probe. (a) Holes. (b) Electrons.

between the icosahedra (10^{-7} to 10^{-6} cm) and hence very small compared with the transit distances. Accordingly the mobilities determined characterize the macroscopic drift and are not the intrinsic mobilities between captures in traps.

For the drift of electrons at room temperature the traps, which are, at a distance of 0.188 eV, closest to the conduction band, dominate, while for the high-mobility holes in the lower valence band the occupied states in the upper valence band (at the same distance of 0.188 eV) acts like a trapping level. On one hand the agreement of these trap ionization energies for electrons and holes explains the obvious similarity of their dispersion spectra. On the other hand the differing electronic behaviour of the two levels is responsible for some differences in detail.

The transport of electrons takes place in the conduction band and is influenced by the electron traps. Electron transport by direct transitions between different electron traps can

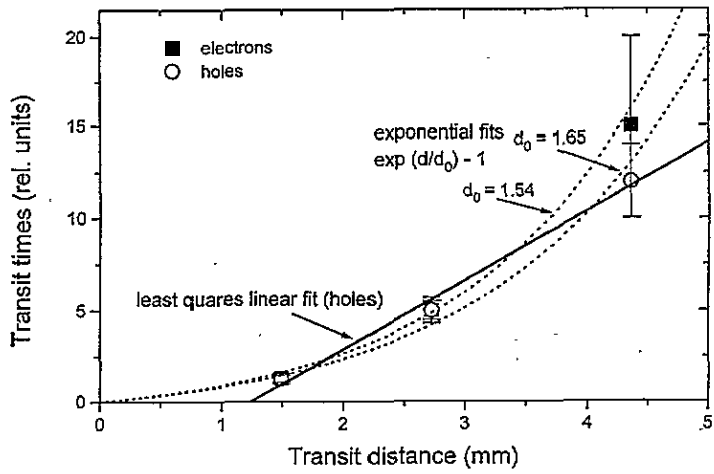

Figure 17. Relative transit times of carriers in the range of multitrapping for different distances from the illuminated surface (see the text). The solid line shows the least-squares linear fit; broken lines show exponential fits.

be largely excluded. The situation for hole transport is different. There are both hopping processes within the upper valence band and high-mobility transport in the lower valence band. For the latter the occupied states in the upper valence band act as hole traps. This is confirmed by the negative photo-effect in the initial range of hole drift. When the occupation density of the upper valence band decreases as a consequence of the drift of holes, the contribution of high-mobility holes in the lower valence band becomes dominant and changes the sign of the photoconduction.

The partial quenching of the conductivity in the case of hole drift makes it evident that the essential conductivity in thermal equilibrium is due to electrons hopping in the upper valence band VB1. For β-rhombohedral boron, at least this disproves the model of hole–bipolaron hopping developed by Howard *et al* [19–22].

From investigations of optical properties it is known that the direct transition of trapped electrons into the conduction band is forbidden. However, in contrast, transitions between the upper valence band, acting as trapping level for free holes, and the conduction band are allowed. This explains why the ratio of retrapping and recombination rate for the electrons is about one order of magnitude larger than for holes. When electrons propagate from the illuminated surface into the bulk, a proportion of them recombine into the upper valence band and this reduces the concentration of unoccupied valence band states. Accordingly the recombination rate for the following electrons decreases, retrapping becomes dominant and the drift length between generation and interband recombination of the electrons increases considerably. In contrast, in the case of drifting holes the upper valence band becomes emptied, the trapping rate for holes in the lower valence band decreases, and the recombination probability increases. As well as multi-trapping in deeper electron traps this is also assumed to be an essential reason for the dispersion curves of electrons extending to much longer times than those of the holes.

The interpretation of the preceding results is at least qualitatively consistent with numerous other experiments, which have led to the band scheme in figure 1. The importance of such experiments for a better qualitative and in particular quantitative understanding of the complex electronic transport properties of the boron-rich structures is obvious. Further experiments depending on temperature, excitation intensity, and excitation energy at much

higher drift fields are in progress.

References

[1] Franz R and Werheit H 1989 *Europhys. Lett.* **9** 145

[2] Franz R and Werheit H 1990 Influence of the Jahn–Teller effect on the electronic band structure of boron-rich solids containing B_{12} icosahedra *AIP Conf. Proc.* **231** 29

[3] Werheit H and Kuhlmann U 1993 *Solid State Commun.* **88** 421

[4] Werheit H, Laux M and Kuhlmann U 1993 *Phys. Status Solidi* b **176** 415

[5] Werheit H 1994 The electronic structure of β-rhombohedral boron and the relation to its physical properties *Proc. 11th. Int. Symp. on Boron, Borides and Related Compounds (Tsukuba, Japan, 1993); Japan J. Appl. Phys.* **10** 66

[6] Szadkowski A and Stankiewicz J 1970 Drift mobility of carriers in boron *Boron* vol 3, ed T Niemyski (Warsaw: PWN Polish Scientific Publishers) p 291

[7] Uno R, Ozawa H and Ishigaki J 1990 Transient photoconduction of β-rhombohedral bulk boron *AIP Conf. Proc.* **231** 130

[8] Werheit H 1983 Boron *Landolt–Börnstein Numerical Data and Functional Relationships in Science and Technology, New Series* Group III, vol 17e, ed O Madelung, M Schulz and H Weiss (Berlin: Springer) p 9

[9] Werheit H, Kristen F and Franz R 1992 *Phys. Status Solidi* b **172** 405

[10] Binnenbruck H, Hausen A, Runow P and Werheit H 1970 *Z. Naturf.* a **25** 1431

[11] Franz R 1990 *Thesis* University of Duisburg

[12] Fisher NE and Willock D J 1992 *J. Phys.: Condens. Matter* **4** 2517

[13] Scher H and Montroll E W 1975 *Phys. Rev.* B **12** 2455

[14] Pfister G and Scher H 1978 *Adv. Phys.* **27** 747

[15] Schmidlin F W 1977 *Phys. Rev.* B **16** 2362

[16] Movaghar B, Murray D W, Donovan K J and Wilson E G 1984 *J. Phys. C.: Solid State Phys.* **17** 1247

[17] Wilson E G 1979 *J. Phys. C: Solid State Phys.* **13** 2885

[18] Young J D, Oliver D W and Slack G A 1969 *Appl. Phys. Lett.* **14** 301

[19] Howard I A, Beckel C L and Emin D 1987 *Phys. Rev.* B **35** 2929

[20] Howard I A, Beckel C L and Emin D 1987 *Phys. Rev.* B **35** 9265

[21] Howard I A, Beckel C L and Emin D 1987 Bipolaron formation in B_{12} and $(B_{11}C)^+$ icosahedra *MRS Symp. Proc.* **97** 177

[22] Emin D 1990 Electronic and vibrational hopping transport in boron carbides *AIP Conf. Proc.* **231** 65